ELSEVIER

Journal of Contaminant Hydrology 30 (1998) 333–362

JOURNAL OF
Contaminant
Hydrology

On water seepage and fast preferential flow in heterogeneous, unsaturated rock fractures

K. Pruess *

Earth Sciences Division, Lawrence Berkeley National Laboratory, University of California, Berkeley, CA 94720, USA

Received 22 August 1996; revised 15 May 1997; accepted 15 May 1997

Abstract

Evidence from a number of field sites suggests that water seepage through fractured unsaturated zones may proceed, in part, by means of fast preferential flow paths. This paper presents conceptual and numerical models which aim at developing an understanding of water seepage behavior in such media, and exploring conditions for fast preferential flow. Water seepage has been numerically simulated in heterogeneous fractures, which were conceptualized as two-dimensional heterogeneous porous media. Flow was found to proceed in dendritic patterns along preferential paths, giving rise to such features as localized ponding and bypassing. Fast preferential flow can occur from 'external' (non-uniform boundary conditions) or 'internal' mechanisms (heterogeneities), or a combination thereof. A most effective condition for fast preferential flow is the presence of sub-horizontal barriers of significant length. Limited parameter variation studies have shown strong dependence of seepage patterns on fracture permeability and applied flow rate. The temporal evolution of seeps proceeds on a vast range of time scales. This casts doubt on the applicability of steady-state concepts for water migration in unsaturated zones of fractured rock where infiltration is episodic. An approximate invariance of seepage behavior was derived for simultaneous space-and-time scaling, suggesting that seepage patterns should appear more vertically elongated as the scale of observation is increased. Numerical simulation experiments have confirmed this invariance, as well as its limits of applicability.

* Corresponding author.

0169-7722/98/$19.00
PII S0169-7722(97)00049-1

1. Introduction

Seepage of water under isothermal conditions in variably saturated media is usually described with Richards' equation

$$\frac{\partial}{\partial t}\theta = \mathrm{div}\left[K\nabla h\right] \tag{1}$$

where t is time, θ is specific volumetric moisture content, K is hydraulic conductivity, and h is hydraulic head. Eq. (1) may be considered an approximate form of the following multi-phase flow equation (Oldenburg and Pruess, 1993)

$$\frac{\partial}{\partial t}\phi S_{\mathrm{l}}\rho_{\mathrm{l}} = \mathrm{div}\left[k\frac{k_{\mathrm{rl}}}{\mu_{\mathrm{l}}}\rho_{\mathrm{l}}\nabla\left(P_{\mathrm{l}} + \rho_{\mathrm{l}}gz\right)\right] \tag{2}$$

Here, ϕ is porosity, S_{l} is liquid (water) saturation, ρ_{l} is liquid density, k is absolute permeability, k_{rl} is relative permeability to liquid phase, g is acceleration of gravity, μ_{l} is viscosity, $P_{\mathrm{l}} = P_{\mathrm{gas}} + P_{\mathrm{cap}}$ is liquid phase pressure, with P_{gas} the (constant) gas phase reference pressure, P_{cap} the capillary pressure, and z is the vertical coordinate (positive upward). Approximations implicit in Richards' equation include that the gas phase acts as a passive bystander during water flow, with negligible pressure changes, and that water density and viscosity are constant. We then have $\theta \approx \phi S_{\mathrm{l}}, K \approx kk_{\mathrm{rl}}\rho_{\mathrm{l}}g/\mu_{\mathrm{l}}$, and $h \approx z + P_{\mathrm{l}}/\rho_{\mathrm{l}}g$. Further implied are all the approximations that are inherent in (multi-phase extensions of) Darcy's law, such as absence of inertial effects, and applicability of relative permeability and capillary pressure concepts. Also implied is volume averaging on some scale, although Eqs. (1) and (2) do not spell out what the spatial scale of volume averaging is.

For heterogeneous media, the hydrologic parameters (k, ϕ, P_{cap}, etc.) are expected to show random spatial variation with certain correlation structures, and Eqs. (1) and (2) are stochastic partial differential equations (PDEs). The present paper focuses on permeability heterogeneity in the fracture plane. This is believed to be the dominant control on seepage behavior, although spatial variability is also expected to be present for fracture porosity, and in the functional relationships between relative permeability, capillary pressure, and liquid saturation. The transient evolution of saturation (or, equivalently, liquid pressure) in response to certain applied boundary conditions, and sinks and sources, will reflect the heterogeneity of the underlying porosity and permeability distribution. For many applications, such as for assessment of contaminant migration and the performance of waste repositories, we are interested not in the spatial and temporal details of flow but only in flow properties averaged over certain scales. A fundamental question then arises: can such averages be derived from an average saturation field $S_{\mathrm{l}}(x,t)$, obtained by solving some simplified form of Eq. (2) with volume-averaged coefficients, or do we need to tackle the much more difficult problem of solving Eq. (2) with detailed representation of heterogeneity, perhaps for many realizations, and then average the results? Noting that the relative permeability and capillary pressure relationships in Eq. (2) usually are highly non-linear, we expect that

flow behavior and saturation distributions calculated by averaging the heterogeneous porosity and permeability fields, and spatially variable boundary and sink/source conditions, may be quite different from averages obtained for ensembles of heterogeneous fields. It has also been shown that volume averaging will in general not only give rise to effective 'upscaled' parameters, but may give rise to the emergence of novel 'effective processes' which do not necessarily have a small-scale counterpart (Pruess, 1994, 1996a,b). Accordingly, we expect that averaging the inputs for Eq. (2) will, in general, not be a viable approach for obtaining averages for the outputs. The analyses presented below will confirm this expectation. As will be shown, averaging of inputs may not only produce poor approximations, but may in fact lead to predictions that qualitatively disagree with observed trends.

The conventional approach for describing seepage of (aqueous or non-aqueous) liquids in partially saturated fractured media employs macroscale continuum concepts (Peters and Klavetter, 1988). Large-scale volume averaging is used for homogenizing heterogeneous fracture and matrix permeabilities, and to average out spatially variable infiltration rates applied at the system boundary, e.g., at the land surface, or at lithologic contacts between porous and fractured units. On the basis of these volume-averaged concepts, water migration along sub-vertical fractures is then typically predicted as proceeding in the form of smooth sheets, and being subject to strong imbibition effects into the partially saturated rock matrix (Nitao and Buscheck, 1991; Wang and Narasimhan, 1993; Eaton et al., 1996).

There is mounting evidence for non-volume-averaged behavior from field sites with thick unsaturated zones. At Yucca Mountain, Nevada, where the water table is approximately 600 m beneath the land surface, analyses of water and rock samples from the unsaturated zone have shown that environmental tracers have migrated to several hundred meters depth in a matter of decades. If water seepage were taking place in volume-averaged fashion, solute transport to such depths would require thousands of years. Elevated levels of ^{36}Cl originating from atmospheric nuclear tests conducted in the 1950s and 1960s were found at several locations in the Exploratory Studies Facility (ESF), at approximately 300-m depth (Fabryka-Martin et al., 1996). The elevated ^{36}Cl levels were in some cases associated with bomb-pulse ^{99}Tc. This and the observation of high levels of bomb-pulse tritium (Yang et al., 1995) add further confirmation to the presence of fast preferential flow paths. At nearby Rainier Mesa, persistent highly localized flow of water from fractures into drifts located above the water table was observed at depths of several hundred meters beneath the land surface (Thordarson, 1965; Lawrence Berkeley Laboratory, 1991; Wang et al., 1993). Typically, only portions of fractures carried water, and the chemical composition of water obtained from fractures was substantially different from that of water samples extracted from the nearby rock matrix. At the Superior mine in Arizona, water inflow from fractures into mine drifts in a partially saturated environment at several hundred meter depth varied with precipitation at the surface, with a lag time of only a few months (D. Chesnut, private communication, 1996). At a field site in the Negev desert, Israel, man-made tracers were observed to rapidly migrate across a thick unsaturated zone of fractured chalk (Nativ et al., 1995). All these observations indicate that in semi-arid environments water is able to migrate downward rather rapidly along localized preferential flow paths

through fracture networks in partially saturated rocks, without being imbibed into the rock matrix. Localized preferential flow of water along non-horizontal fractures has also been observed in laboratory experiments (Nicholl et al., 1993, 1994; Glass, 1993; Geller and Pruess, 1995).

Recognizing that fast water flow along localized preferential paths may play an important role in unsaturated fractured rock, several researchers have suggested to abandon continuum-type treatments based on PDEs such as Eq. (1), and have proposed to instead conceptualize unsaturated flow in heterogeneous fractured media as a stochastic distributions of localized seeps (Gauthier et al., 1992; Gauthier, 1994; Chesnut, 1992, 1994). In the cited references, distributions of seeps were introduced in an ad hoc fashion. The objective of the present work is to propose and explore a continuum-based mechanistic model for localized seeps and their properties, and thereby contribute to a better understanding of flow and transport in unsaturated fractured media. We begin with a general discussion of conditions that are conducive to the development of fast preferential flows in unsaturated media. We then introduce our conceptualization of fractures as two-dimensional heterogeneous porous media (Pruess et al., 1990a; Pruess and Tsang, 1990). It is assumed that Richards' equation and its implied approximations, such as applicability of relative permeability and capillary pressure concepts, are valid for such media on a scale of 0.1–1 m. High-resolution numerical simulations of unsaturated flow are performed in which we explicitly consider fracture heterogeneity on a sub-meter scale. The TOUGH2 code (Pruess, 1991) was used for the simulations, augmented with a set of preconditioned conjugate gradient solvers (Moridis and Pruess, 1995) and a special fluid property module 'EOS9' for Richards' equation (Pruess, 1994).

2. Conditions for fast preferential flow

We are primarily interested in fast preferential flow in the downward direction, driven by gravity force. In a continuum model of flow, the seepage (pore) velocity v for an applied volumetric flux (Darcy velocity) u in a medium initially at irreducible liquid saturation S_{lr} is given by

$$v = \frac{u}{\phi(S_{\mathrm{l}} - S_{\mathrm{lr}})}. \tag{3}$$

Note that the velocity of a conservative tracer would be expected to be smaller than the velocity given by Eq. (3). A tracer would diffuse into regions with immobile water, so that its velocity would be intermediate between v of Eq. (3) and $u/\phi S_{\mathrm{l}}$, and may be closer to the latter value. Eq. (3) indicates that fast preferential flow can occur in regions with (a) larger Darcy velocity, (b) smaller flow porosity, (c) smaller effective liquid saturation $S_{\mathrm{e}} = (S_{\mathrm{l}} - S_{\mathrm{lr}})$. Several different conditions can independently or concurrently give rise to such effects.

Suppose that infiltration at the land surface is applied at constant rate in a spatially uniform manner. Locally high values of Darcy velocity can be generated from suitable heterogeneities of the medium. Sub-horizontal regions of low effective permeability can

act as funnels to divert flows sideways, diminishing downward flow in some regions while concentrating it in others. Field observations in heterogeneous soils have shown that such flow 'funneling' can give rise to local enhancements in Darcy velocity by factors as large as 10–100 in comparison to uniformly distributed seepage (Kung, 1990a,b). To be effective in funneling flow, the low-permeability regions need to have considerable lateral extent. Features that can provide such funneling include clay or silt lenses, capillary barriers at sloping interfaces between fine and coarse soil layers, or at lithologic contacts, fracture terminations, and asperity contacts in fractures. Favorable conditions for enhancing the seepage velocity for a given Darcy flux exist in regions of locally high vertical permeability, such as fractures, where sufficient effective permeability for flow will be available at small effective water saturations. Fracture networks also provide small flow porosity and associated enhanced seepage velocity.

The conditions for fast preferential flow discussed so far are 'internal' to the medium, deriving from a particular structure of heterogeneities. In addition there is an 'external' mechanism that can produce localized seepage simply by means of non-uniform infiltration applied at the land surface boundary. For example, in regions with topographic relief, runoff may funnel and focus much infiltration into topographic lows. Fractures or faults extending to (near) the land surface may accept an above-average amount of precipitation.

Numerical simulation is used here as a means to investigate occurrence and behavior of both internally and externally induced preferential flow in heterogeneous fractures.

3. Heterogeneous fractures

Natural rock fractures are expected to encompass a vast variety of aperture distributions. The present work focuses on 'small-aperture' fractures in hard rocks, such as tuffs, basalts, granites, or graywackes. Aspects of fracture aperture distribution that are believed to be essential for replicating natural features include (a) the presence of asperity contacts, where the fracture walls touch, (b) a more or less gradual change towards larger apertures away from the asperities, (c) small-scale fracture wall roughness, and (d) finite-size spatial correlation length among apertures (Wang and Narasimhan, 1985; Pruess and Antunez, 1995).

A synthetic heterogeneous permeability field that can represent a fracture is obtained by means of the turning bands method, as implemented by Tompson (1989). This method requires a lognormal distribution of 'permeability modification coefficients' (see below), given by

$$f(\zeta) = \frac{1}{\zeta\sigma\sqrt{2\pi}} \exp\left(- \frac{\left(\ln(\zeta) - \langle \ln(\zeta) \rangle^2\right)}{2\sigma^2} \right). \tag{4}$$

The particular lognormal distribution shown in Fig. 1 corresponds to parameters of $\langle \ln(\zeta) \rangle = 1$, standard deviation $\sigma = 1.5$. Using 10,000 ζ-coefficients randomly picked from the distribution Eq. (4), a two-dimensional rectangular grid of 100×100 coefficients ζ_{ij} is then generated as a spatially-correlated stochastic field. An exponential

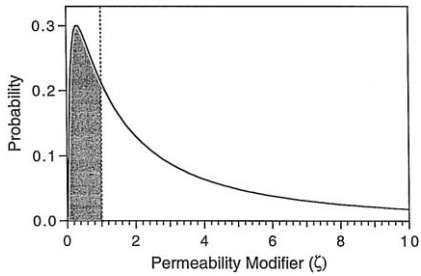

Fig. 1. Lognormal distribution of permeability modification coefficients for synthetic fracture. The shaded region, having an area of 0.264, ends up representing asperity contacts after application of the shift given by Eq. (5).

spatial correlation structure is used with spatial correlation lengths of 1 grid unit in the horizontal direction, 0.5 in the vertical. The lognormal distribution has zero probability for the value $\zeta = 0$, hence cannot represent asperity contacts. To achieve the desired asperity contacts (regions of zero permeability), the lognormally distributed coefficients ζ_{ij} are 'shifted' according to

$$\zeta_{ij} \rightarrow \zeta'_{ij} = \max\left(\zeta_{ij} - \Delta, 0\right). \tag{5}$$

The ζ'_{ij} coefficients are then attached to a finite difference grid of $100 \times 100 = 10{,}000$ square blocks, each of which is assigned a permeability $k_{ij} = \zeta'_{ij} \times k_{\mathrm{ref}}$, where reference permeability is typically chosen as $k_{\mathrm{ref}} = 10^{-9}$ m^2. The capillary pressure functions are scaled along with permeability on a grid-block-by-grid-block basis according to $P_{\mathrm{cap}} \rightarrow P'_{\mathrm{cap}} = P_{\mathrm{cap}}/(\zeta'_{ij})^{1/2}$ (Leverett, 1941); the same relative permeability functions are used in all grid blocks regardless of absolute permeability. A space discretization of 10,000 grid blocks was chosen because this permits a fairly detailed representation of spatially-correlated heterogeneity, while leading to a computational problem that is still easily handled on workstations. Grid spacing was taken to be 0.2 m in most simulations, based on laboratory experiments which have shown that macroscale continuum concepts, such as relative permeability and capillary pressure, are applicable to rough-walled fractures on a decimeter scale (Persoff and Pruess, 1995). With these parameter choices, a typical fracture size is 20×20 m^2, which is reasonable for Rainier Mesa (Thordarson, 1965), and is at the high end of but not incompatible with fracture sizes observed at Yucca Mountain (L. Anna, private communication, 1996). The representation of a fractured medium as a single planar fracture for purposes of flow modeling is not as restrictive as it may seem. Indeed, such a modeling approach can be used to approximate stochastic distributions of flow channels in networks of intersecting fractures (Tsang and Tsang, 1987).

For the flow simulations reported here the shift Δ was chosen as 1, which resulted in a fraction of 26.4% of the permeability modifiers ζ'_{ij} being equal to 0, corresponding to asperity contacts (Fig. 2). This fraction of fracture wall contact area is considered reasonable, based on analyses of fracture wall coatings from Yucca Mountain (Wang and Narasimhan, 1993). For a reference permeability of 10^{-9} m^2, the corresponding parallel-plate hydraulic aperture (Witherspoon et al., 1980) is $b = (12k)^{1/2} = 0.1095$

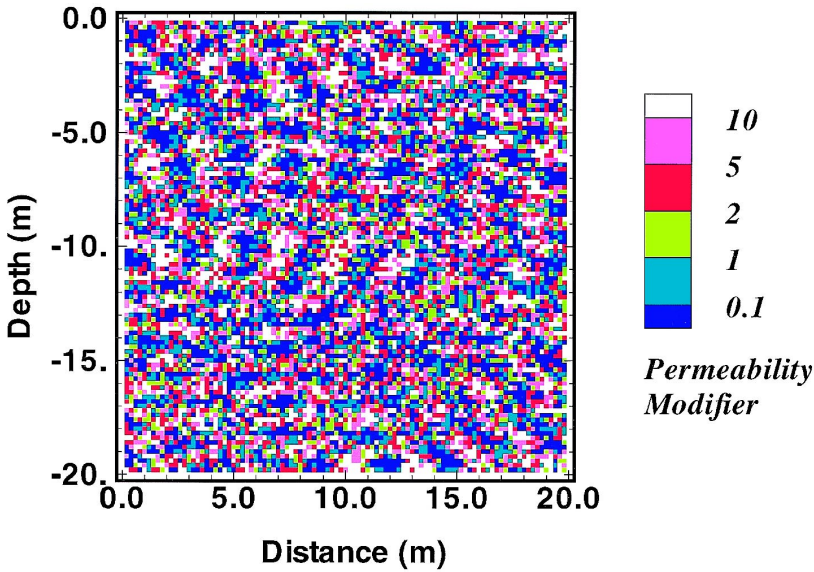

Fig. 2. Permeability modifiers for synthetic heterogeneous fracture.

mm. It is well known that in natural rough-walled rock fractures the 'volumetric aperture' (defined as fracture void volume per unit surface area) is considerably larger than the hydraulic aperture, often by orders of magnitude (Abelin et al., 1987). This is explained by the fact that fracture permeability is controlled by the smallest apertures (largest flow resistance), while fracture void volumes are dominated by the largest apertures. We do not use a parallel-plate concept, but instead model the fracture as a two-dimensional heterogeneous porous medium.

Seepage behavior is determined, generally speaking, by an interplay between permeability heterogeneity, capillary pressure and relative permeability effects, and spatial variations in volumetric aperture. Permeability heterogeneity and associated variations in strength of capillary pressures are expected to be the dominant control on seepage behavior. Accordingly, we neglect possible spatial variations in fracture volumetric aperture in this study, except that in regions of zero permeability apertures were assumed to be zero. The fracture is represented as a 10 mm thick heterogeneous porous medium of 'large' permeability. Intrinsic porosity of the fracture is chosen as $\phi = 0.35$, corresponding to a volumetric aperture of 3.5 mm. (Note that the same volumetric aperture could have been achieved with different combinations of thickness and porosity, e.g., 20 mm thickness and $\phi = 0.175$, etc.) The volumetric aperture is larger than the hydraulic aperture by a factor of 32.0, which is consistent with data given by Abelin et al. (1987) who found that for fractures at Stripa the volumetric apertures exceeded hydraulic apertures by factors of from 17.6 to 137.5. For a reference permeability of $k_{\mathrm{ref}} = 10^{-9}$ m^2, the permeability-thickness product of the fracture is 10^{-11} m^3, or 10 darcy m. Analysis of barometric pressure propagation suggests that such values are

reasonable for fractures in welded tuffs at Yucca Mountain, (R. Ahlers, private communication, 1996).

Matrix permeability of unfractured welded tuffs is typically of order 10^{-18} m^2 (1 microdarcy) or lower. This is many orders of magnitude smaller than typical permeabilities in the fracture plane. A number of fully 3-D calculations were performed to quantify the importance of water imbibition into wall rocks. The results confirmed expectations that rock matrix permeability has little impact on seepage behavior over shorter time periods (days), although imbibition into the rock matrix may be an important long-term effect. This paper is mainly concerned with flow of injected water in the fracture plane over relatively short time periods (days), and matrix permeability was neglected in most simulations

4. Flow simulations

The flow simulations were carried out by injecting water at various time-independent rates at the top of the fracture shown in Fig. 2. In most simulations, injection was made over different 1 m intervals, corresponding to five neighboring grid blocks, centered at distances of, respectively, 6.5, 8.5, 10.5, and 12.5 m from the left boundary of the fracture. Injection at a prescribed rate into a heterogeneous medium raises some non-trivial issues. It would not be acceptable to simply distribute the desired injection rate uniformly over the grid blocks adjacent to the injection boundary. Indeed, because of the strong heterogeneities present some of the injection blocks may be unable to take a $1/5$ share of the total injection rate without large and unphysical pressure excursions. We accomplish injection by attaching an additional injection grid block of 1 m horizontal length and 'average' permeability (see below) to the top of the fracture at the desired injection interval. As water is injected at a prescribed rate into this block, water saturation will increase and outflow into the fracture blocks beneath the injection block will take place. The outflow will in general partition non-uniformly among the fracture blocks. After steady flow conditions are reached near the injection interval, the injection block will remain in conditions of constant water saturation and capillary pressure. Thus, after a rapid initial transient, the boundary conditions at the top of the fracture will be

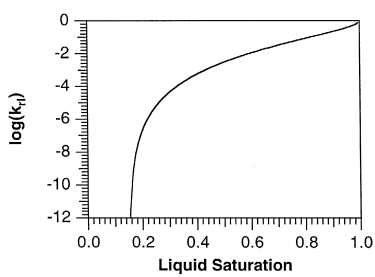

Fig. 3. Relative permeability function.

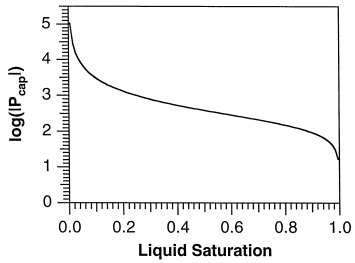

Fig. 4. Capillary pressure function for reference permeability of $k = 10^{-9}$ m^2. Capillary pressure is in Pa.

constant capillary pressure over the injection interval, even though the boundary condition specified for the injection block is 'constant rate.'

Lateral boundaries were 'no flow,' and at the bottom a unit head gradient boundary condition was imposed. This is the condition that would develop, on average, if we had specified the fracture to be of much larger vertical length, situated 'far' above the water table (beyond the capillary fringe). In other words, the bottom unit head gradient boundary condition enables us to model flow in a fracture of finite vertical extent, without unphysical finite-size effects propagating upwards from the bottom boundary. Recent theoretical and experimental work suggests that relative permeability and capillary pressure behavior of fractures is similar to that of highly permeable media with intergranular porosity (Pruess and Tsang, 1990; Firoozabadi and Hauge, 1990; Persoff and Pruess, 1995). Accordingly, we used the customary van Genuchten correlations, with parameters chosen as for coarse sands (see Figs. 3 and 4; van Genuchten, 1980; Pruess, 1996b). Initial water saturation in the fracture was specified at the irreducible level of $S_l = S_{lr} = 0.15$, so that all additional water introduced into the fracture would be

Table 1
Parameters for heterogeneous fracture flow simulations

Reference permeability	$k_{ref} = 10^{-9}$ m^2
Porosity	$\phi = 0.35$
Relative permeability	
van Genuchten function (1980): $k_{rl} = \sqrt{S^*}\{1-(1-[S^*]^{1/\lambda})^{\lambda}\}^2$	$S^* = (S_l\text{-}S_{lr})/(1\text{-}S_{lr})$
Irreducible water saturation	$S_{lr} = 0.15$
Exponent	$\lambda = 0.457$
Capillary pressure	
van Genuchten function (1980): $P_{cap} = -(\rho_w g/a)([S^*]^{-1/\lambda}-1)^{1-\lambda}$	$S^* = (S_l\text{-}S_{lr})/(1\text{-}S_{lr})$
Irreducible water saturation	$S_{lr} = 0.0$
Exponent	$\lambda = 0.457$
Strength coefficient	$a = 50$ m^{-1}
Initial water saturation	$S_l = 0.15$
Water density[a]	998.3 kg/m^3
Water viscosity[a]	1.00×10^{-3} Pa s
Water compressibility[a]	4.55×10^{-10} Pa^{-1}

[a]Corresponding to ambient temperature and pressure conditions of $T = 20$°C, $P = 1$ bar.

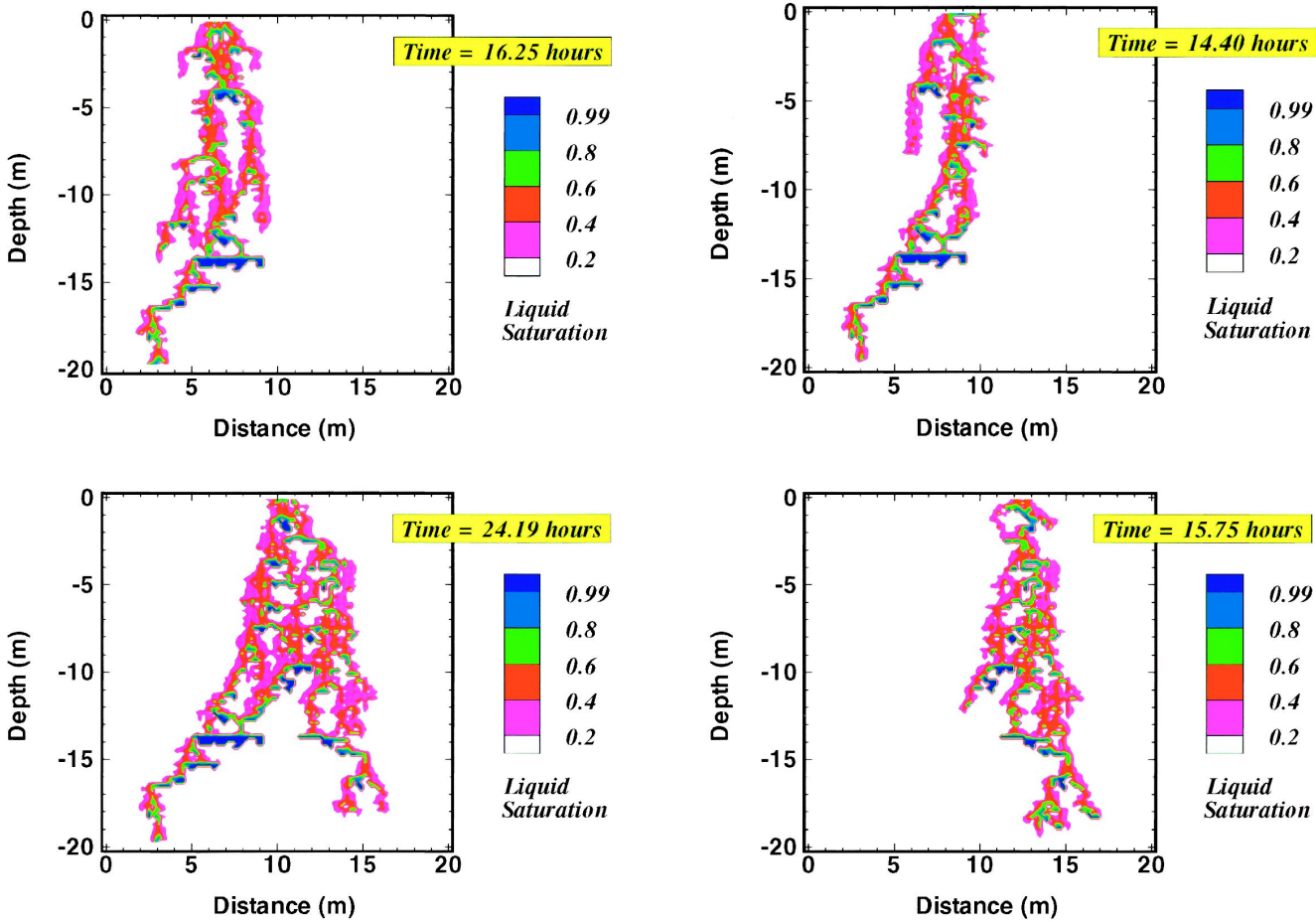

Fig. 5. Liquid seeps shown at the time of breakthrough at a depth of -19.5 m. Water is injected at a constant rate of 10^{-3} kg/s over a 1 m interval at the top of the heterogeneous fracture of Fig. 2. The injection interval is centered at different distances from the left boundary, namely, 6.5 m (top left), 8.5 m (top right), 10.5 m (bottom left), and 12.5 m (bottom right). Reference permeability is 10^{-9} m^2.

mobile. A smaller value for the parameter S_{lr} was specified in the capillary pressure as compared to the relative permeability function, to avoid the unphysical behavior of $P_{cap} \to -\infty$ as $k_{rl} \to 0$. A summary of problem specifications appears in Table 1.

For comparison, we also simulated injection into a homogeneous fracture, with absolute horizontal and vertical permeabilities assigned to average values of those for the heterogeneous fracture. Average permeability was 'measured' by numerically simulating a single-phase flow problem, as follows. Fully saturated constant pressure conditions were specified at the top and bottom boundaries of the heterogeneous fracture, and a flow simulation was run to steady state. Vertical permeability was then calculated from the steady flow rate and applied pressure drop, using Darcy's law. An analogous procedure was applied to obtain horizontal permeability, specifying fully saturated constant pressure boundary conditions at the left and right edges of the heterogeneous fracture. Values of $k_h = 0.69 \times k_{ref}$, $k_v = 0.36 \times k_{ref}$ were obtained for the horizontal and vertical permeabilities, respectively, which were then used in the homogeneous fracture simulations.

5. Localized infiltration

Fig. 5 shows simulated seeps in the heterogeneous fracture for a reference injection rate of 10^{-3} kg/s, applied over different 1 m intervals at the top of the fracture, at the time of breakthrough at -19.5 m depth. The seeps are quite different in appearance but share common features. Flow generally proceeds in narrow vertical or sub-vertical fingers. Several flow paths can develop from localized injection. These can either merge again or remain separate as water continues to migrate downward. Perched water bodies develop at asperity contacts which are associated with significant effects of bypassing and lateral displacements. Breakthrough times at -19.5 m depth vary from 14.40 to 24.19 h, corresponding to average velocities of seep advancement from 0.81 to 1.35 m/h (see Table 2). Lateral displacement at breakthrough over the 19.5 m vertical migration distance varies from -7.5 m to $+1.0$ m.

For comparison we simulated infiltration in a homogeneous fracture. Injection over a 1-m interval produces a featureless seep in which water migrates straight downward under gravity, with lateral broadening due to capillary effects (Fig. 6). Breakthrough at a depth of -19.5 m occurs after 23.81 h, corresponding to an average seepage velocity of 1.22 m/h. When infiltration is applied uniformly over the entire 20-m wide top

Table 2
Simulated results for seeps in heterogeneous fracture

Seep	#1	#2	#3	#4
Injection point distance (m)	6.5	8.5	10.5	12.5
Breakthrough time at 19.5 m depth (h)	16.25	14.40	24.19	15.75
Average seep velocity (m/h)	1.20	1.35	0.81	1.24
Lateral displacement at breakthrough (m)[a]	−3.5	−5.5	−7.5	+1.0

[a] Positive when displacement is to the right of the injection point, negative otherwise.

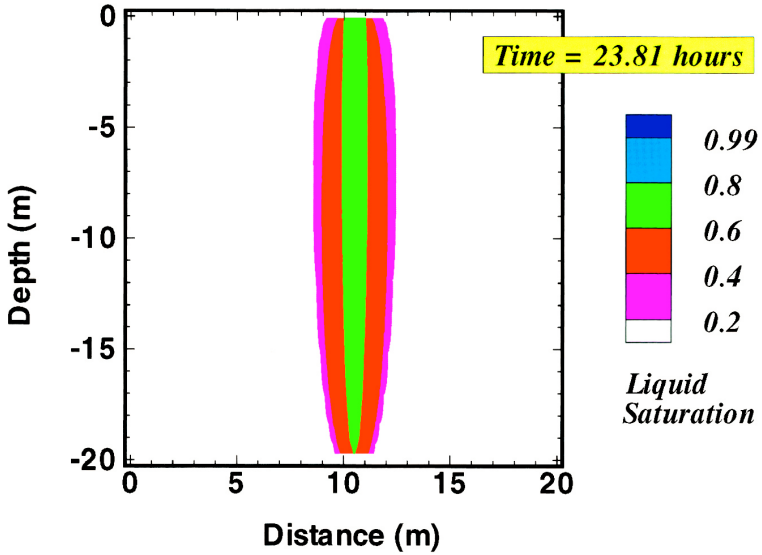

Fig. 6. Liquid seep at time of breakthrough for injection into a homogeneous fracture at a constant rate of 10^{-3} kg/s over a 1 m interval at the top, centered at 10.5 m. Horizontal and vertical permeability are, respectively, 0.69×10^{-9} m^2 and 0.36×10^{-9} m^2, corresponding to the average permeabilities of the heterogeneous fracture of Fig. 2.

boundary of a homogeneous fracture, a uniform seepage field results with breakthrough at -19.5-m depth occurring after 119.08 h.

There is a general tendency for the vertical advancement of seeps to slow down with time (Fig. 7). However, the behavior of seeps #1 and #2 near breakthrough shows that this is not always the case. Seepage velocities in the heterogeneous and homogeneous cases are similar; due to the localized infiltration they are increased by factors from 4.9

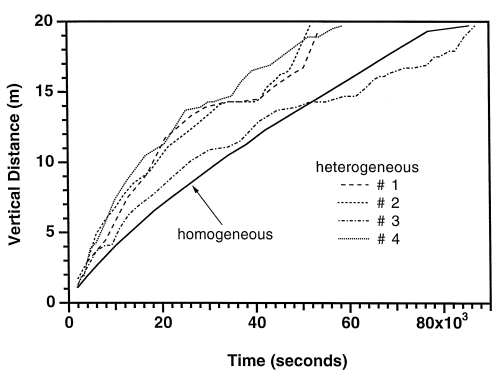

Fig. 7. Vertical advancement of seeps with time for injection into a homogeneous and a heterogeneous fracture. The heterogeneous cases labeled #1 through 4 correspond to the sequence of four seeps shown in Fig. 5, with injection intervals centered at 6.5, 8.5, 10.5, and 12.5 m, respectively.

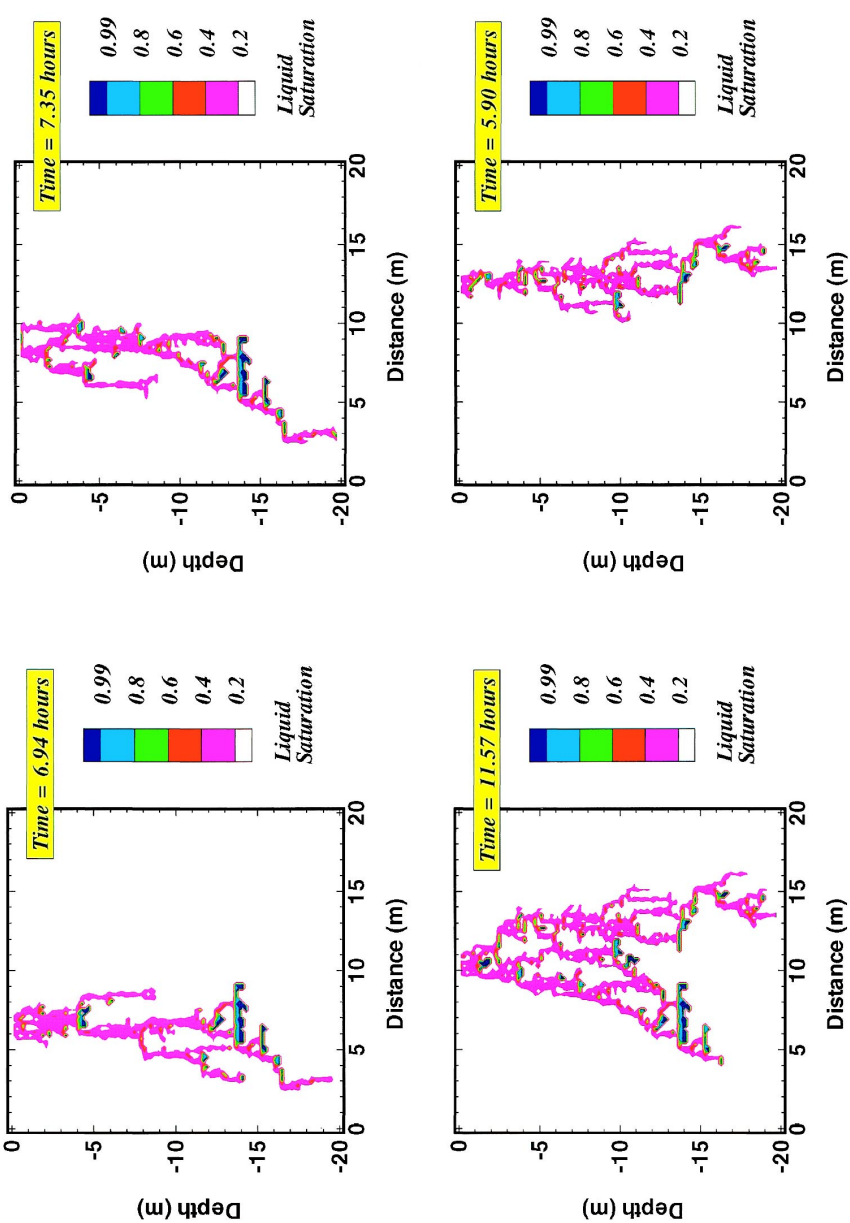

Fig. 8. As Fig. 5, but reference permeability of 10^{-7} m^2.

to 8.3 in comparison to the case where infiltration is applied uniformly across the entire top of the homogeneous fracture. Three of the four heterogeneous seeps advance somewhat faster than the homogeneous seep. Seep #3 is an exception; it is the slowest to break through because it splits into two separate parts, both of which carry comparable amounts of fluid. Detailed inspection reveals that average width of the seeps generally increases with vertical migration distance, and that average liquid saturations stabilize after early-time transients at values close to that for the homogeneous seep (Pruess, 1996c).

A number of fully three-dimensional simulations were conducted to assess effects of water imbibition into the rock matrix. Wall rock properties were taken from measurements for welded tuff sample G4-6 from Yucca Mountain (Peters et al., 1984), which has a matrix permeability of 1.9×10^{-18} m^2. In all cases the seepage patterns were indistinguishable from the cases without matrix flow shown in Fig. 5; however, breakthrough times were approximately 6% longer. Thus, for the time scales of hours to days considered here, effects of matrix imbibition are small and may be neglected.

6. Dependence on permeability, capillary effects, and flow rate

At a two orders of magnitude larger reference permeability of 10^{-7} m^2 the seeps have generally smaller water saturations, because the imposed flow rate can be carried at lower relative permeability (Fig. 8). There is also less broadening of the seeps, due to the weaker capillary pressures. Both effects diminish the amount of water that needs to be injected to achieve breakthrough at the bottom. Vertical migration velocities for the four seeps are increased by factors of 2.34, 1.96, 2.09, and 2.67 in comparison to the $k = 10^{-9}$ m^2 case. It is seen that the speedups are quite different for the different seeps; the seep that is fastest at $k = 10^{-9}$ m^2 is only the third to break through at $k = 10^{-7}$ m^2. Seep #3 broke through at a lateral displacement of -7.5 m for $k = 10^{-9}$ m^2, whereas at $k = 10^{-7}$ m^2 lateral displacement at breakthrough is $+3.0$ m. From these comparisons it is obvious that the same underlying heterogeneity structure can produce quite different seeps at different values of reference permeability.

Capillary effects remain quite significant even at a large reference permeability of $k = 10^{-7}$ m^2, as can be seen by arbitrarily setting $P_{\mathrm{cap}} = 0$ for $k = 10^{-7}$ m^2 (keeping only the gravity force term in Eq. (2)), which gives rise to much narrower fingering flow (Fig. 9). In addition overall shape and direction of the seep is affected; neglecting capillary pressure effects changes the lateral displacement at breakthrough from $+1.0$ m to $+4.8$ m. Breakthrough time is shortened by 7.0%; the surprisingly small magnitude of this effect is explained by the observation that on the different course taken for $P_{\mathrm{cap}} = 0$, the seep actually develops another ponded region (near -18 m depth), which slows its vertical propagation. In general we expect that vertical advancement of seeps may be considerably faster when capillary pressures are weak.

Fig. 9. Liquid seeps at breakthrough at -19.5 m depth for injection at a constant rate of 10^{-3} kg/s over a 1 m interval at the top, centered at 12.5 m. Reference permeability is 10^{-9} m^2 (top) and 10^{-7} m^2 (middle and bottom). For the seep shown at the bottom, capillary pressure effects were neglected.

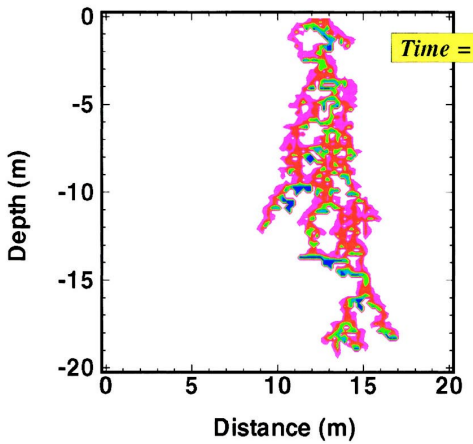

$k = 1.e\text{-}9\ m^2$

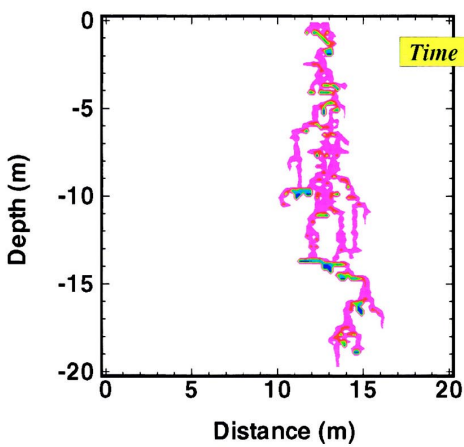

$k = 1.e\text{-}7\ m^2$

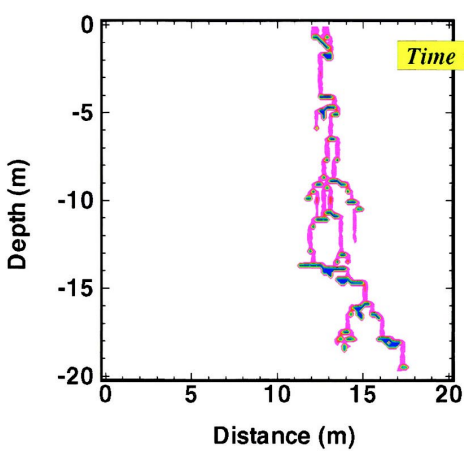

$P_{cap} = 0$

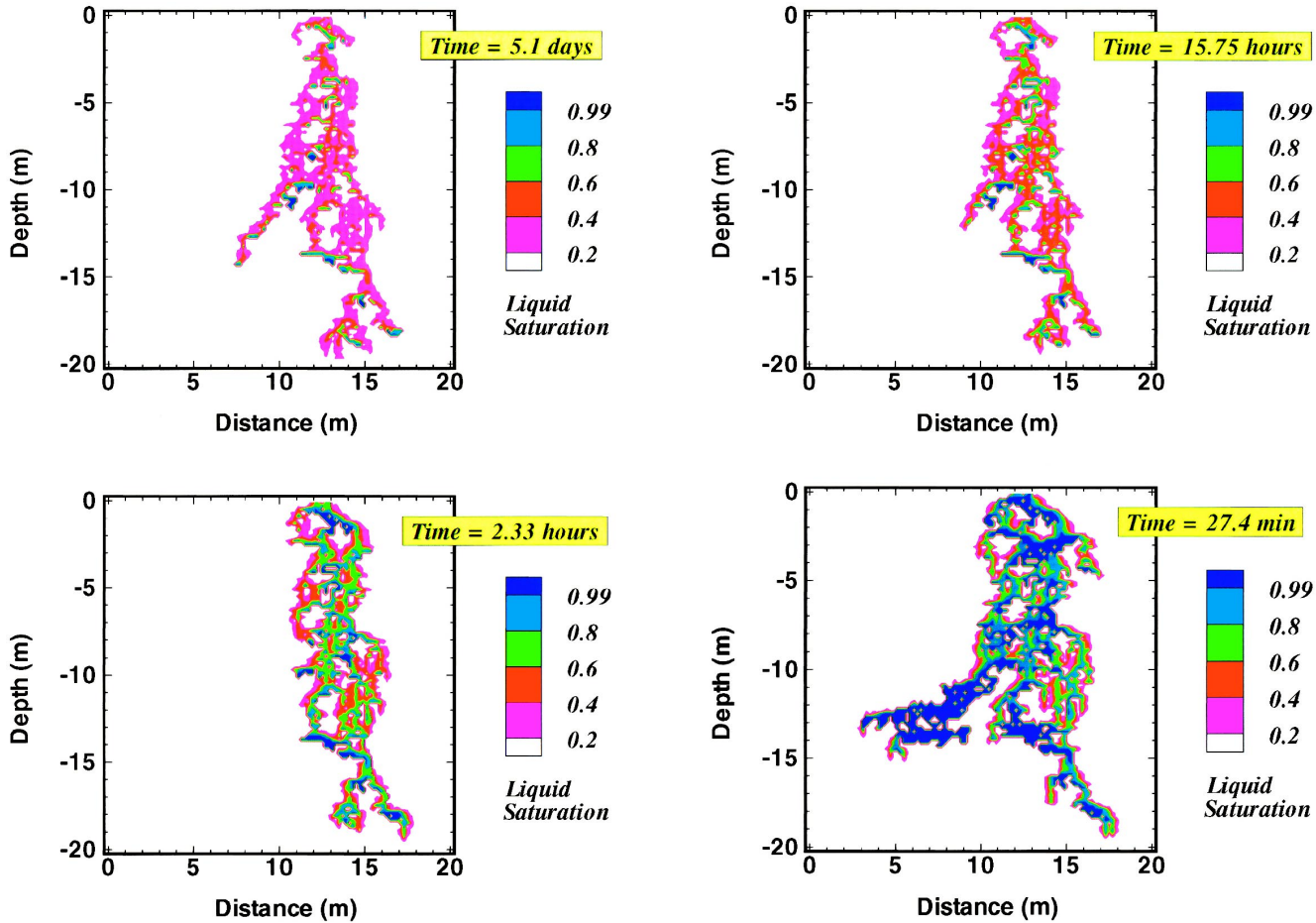

Fig. 10. Liquid seeps at time of breakthrough at -19.5 m depth for injection at four different rates over a 1 m interval at the top, centered at 12.5 m. Injection rates are 10^{-4} kg/s (top left), 10^{-3} kg/s (top right), 10^{-2} kg/s (bottom left), and 10^{-1} kg/s (bottom right). Reference permeability is 10^{-9} m^2.

While breakthrough at the bottom boundary occurs in a matter of hours, calculations for longer times (not shown) indicate that the seeps continue to evolve over a hierarchy of time scales. Even when neglecting the small matrix permeability and considering flow in the fractures only, seeps for constant-rate infiltration continue to change over time periods of years and decades (Pruess, 1996c). Yet slower transient processes will be introduced when matrix permeability is taken into account. Under field conditions infiltration rates at the land surface would be expected to show considerable variability on much shorter time scales, suggesting that naturally occurring seeps should not as a rule be expected to having attained steady-state flow conditions.

Fig. 10 illustrates the rate dependence of a particular seep. As injection rates are increased by successive factors of 10, from 10^{-4} kg/s to 10^{-1} kg/s, water saturations generally become larger. There are also striking changes in appearance. Increasing the injection rate tends to diminish lateral fingering flow, with the $q = 10^{-2}$ kg/s seep most closely resembling the appearance observed for a homogeneous medium (cf. Fig. 6). When injection rate is increased beyond 10^{-2} kg/s, lateral branching again becomes stronger. This indicates that heterogeneous unsaturated media tend to behave most strongly heterogeneous at large and small water saturations, while behaving less heterogeneous at intermediate water saturations (Birkholzer and Tsang, 1996).

7. Distributed infiltration

In the simulations presented so far, localized seepage occurred because of conditions that are external to the flow system, namely, infiltration at the top boundary was applied

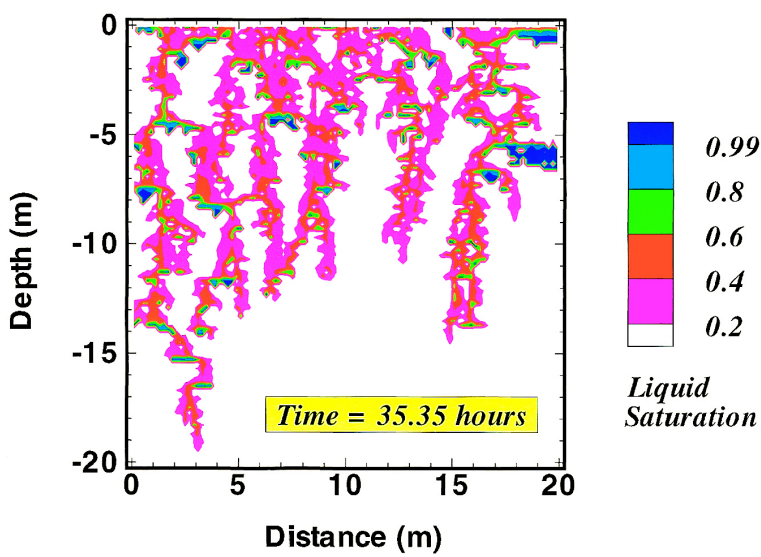

Fig. 11. Liquid seepage at the time of breakthrough at a depth of −19.5 m for water injection at a constant rate of 10^{-3} kg/s over the entire top of the fracture.

in a non-uniform, localized manner. We proceed now to considering internal conditions of the medium that produce localized preferential seeps from an applied spatially uniform infiltration.

When an injection rate of 10^{-3} kg/s is applied uniformly across the top of the heterogeneous fracture of Fig. 2, at a reference permeability of 10^{-9} m^2, breakthrough at -19.5 m depth occurs after 35.35 h. This represents a considerable enhancement of

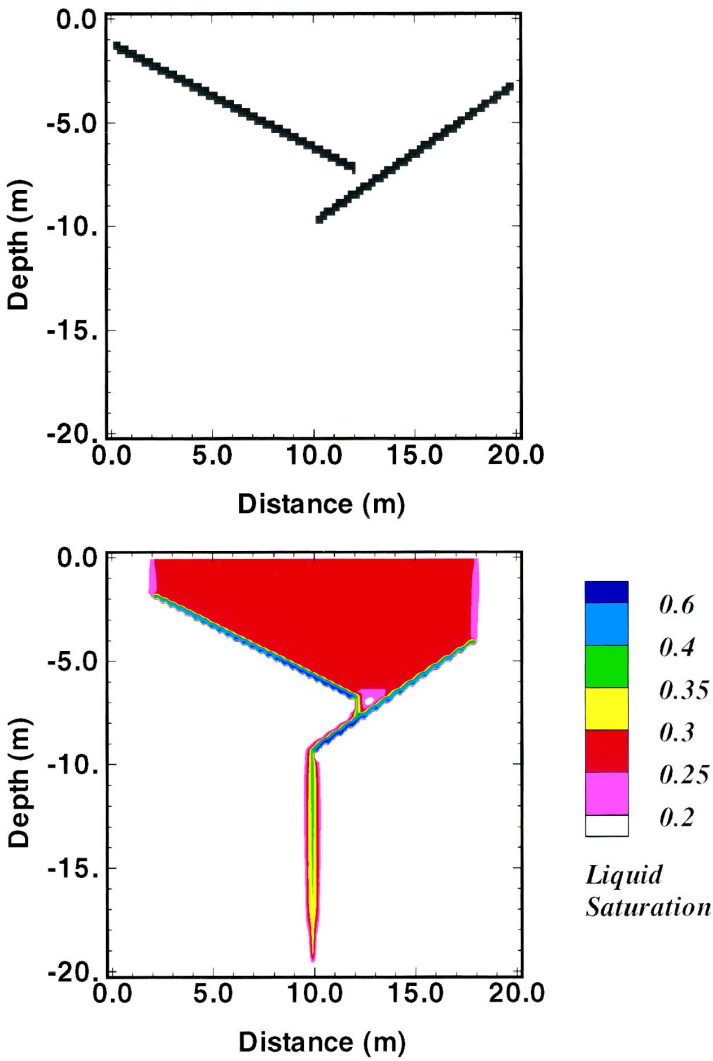

Fig. 12. Sub-horizontal impermeable obstacles forming a funnel structure in an otherwise homogeneous fracture (top), and seepage pattern at breakthrough time for injection of 10^{-3} kg/s over a 16 m wide interval centered at the top of the fracture (bottom).

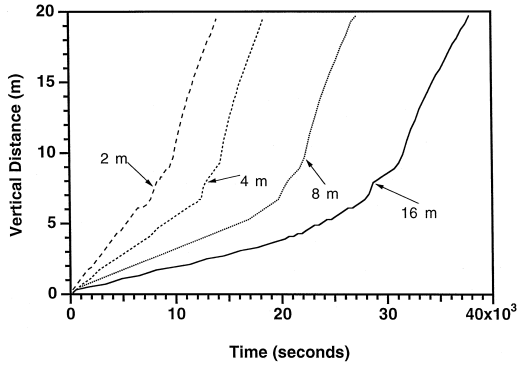

Fig. 13. Vertical advancement of seeps in the funnel-like heterogeneity structure of Fig. 12, for injection of 10^{-3} kg/s over different length intervals centered at the top of the fracture.

seepage velocity (by a factor of 3.4) relative to the homogeneous case. Fig. 11 shows that the enhancement is caused by (a) partial exclusion of flow from portions of the fracture plane due to asperity contacts, and (b) preferential channeling of flux, through an interplay of absolute permeability and capillary pressure effects, into some seeps at the expense of others.

Even stronger localization of seepage and faster flow can occur when longer-range sub-horizontal heterogeneity features are present. Consider the heterogeneity structure shown in Fig. 12, where two sub-horizontal regions of low permeability (assumed zero for simplicity) and large spatial extent are embedded in a fracture plane with otherwise homogeneous permeability, which was chosen here as 10^{-7} m^2. It is obvious that infiltration applied at the top boundary will pond atop the obstacles and be diverted sideways, until it is eventually funnelled into a narrow channel beneath them.

Simulations were performed in which a total infiltration rate of 10^{-3} kg/s was applied over different portions of the top boundary of the fracture. The infiltration intervals were centered at 10 m distance, and ranged in length from 2 m to 16 m. Fig. 12 shows the saturation distribution for infiltration over 16 m length at the time of breakthrough. The vertical advance of seeps over time when infiltration is applied over different length intervals is shown in Fig. 13; results are summarized in Table 3.

After infiltration is started, nearly steady flow conditions are quickly established beneath the infiltration boundary. Average water saturations in this region approach

Table 3
Seepage behavior in the heterogeneous fracture of Fig. 12

Length of infiltration boundary (m)	2	4	8	16
Pore velocity above obstacles (m/h)	3.34	1.93	1.11	0.639
Pore velocity below obstacles at time of breakthrough (m/h)	8.10	8.15	6.72	5.28
Velocity enhancement factor	2.4	4.2	6.1	8.3

constant values, being larger for larger Darcy velocity (smaller length of the infiltration boundary). Water ponds atop the impermeable obstacles, is then diverted sideways, and forms a fast narrow seep beneath the permeable break. For the 16 m long infiltration boundary, the infiltration front has only descended to a depth of -6.72 m at the time the fast seep breaks through at -19.5 m depth. Thus, seepage from the top boundary has not yet reached the obstacles along their entire length, which explains the presence of a region of low water saturation near the permeability break in Fig. 12. As was to be expected, the results as given in Table 3 show that enhancement of seepage velocities from this funneling process becomes stronger when flow is gathered from a longer infiltration boundary. While Darcy velocity above the obstacles is inversely proportional to the length of the infiltration boundary, pore velocity decreases more slowly with increasing length of the infiltration boundary, because for smaller Darcy velocity average water saturation also becomes smaller (see Eq. (3)). This is one reason why velocity enhancement increases less than proportional with the length of the infiltration boundary. Another reason is that for the longer infiltration boundaries, flow in the funneling region is not yet steady at the time of seep breakthrough, so that pore velocities below the obstacles are less for the 8 and 16 m infiltration boundaries (see Table 3). For a system with greater vertical dimension beneath the funneling region, flow in the funnel would be closer to steady at the time of breakthrough, and seepage enhancement factors would increase more strongly for longer infiltration boundaries.

It is obvious that the presence of long-range impermeable obstacles in the fracture plane diminishes average permeability to single-phase flow in the vertical direction. At the same time it increases the rate of downward advancement of unsaturated seeps. Thus we have the remarkable situation that unsaturated seepage can actually proceed faster in a medium with lower average permeability.

8. Behavior under space and time scaling

In connection with waste isolation problems, an assessment of water seepage in heterogeneous fractures is often required for space and time scales far larger than what is accessible through laboratory experimentation and field observation. It is of interest, therefore, to examine the dependence of seepage behavior on the space and time scales involved (Geller and Pruess, 1995; Pruess, 1996a). This can be conveniently done by considering a discretized version of Eq. (2). Using integral finite differences for space and first-order finite differences for time, a space-and-time discretized version of Eq. (2) for an arbitrary reservoir subdomain (grid block) n can be written as follows (Pruess, 1991)

$$\Delta M_n = \frac{\Delta t}{V_n} \sum_m A_{nm} F_{nm} + \frac{\Delta t}{V_n} Q_n. \tag{6}$$

Here, ΔM_n is the change in the accumulation term over time step $\Delta t = t^{k+1} - t^k$,

$$\Delta M_n = (\phi S_l \rho_l)_n^{k+1} - (\phi S_l \rho_l)_n^k. \tag{7}$$

V_n is the volume of the grid block, and A_{nm} is the interface area between grid blocks n and m. The summation in Eq. (6) extends over all grid blocks m that are connected to n. F_{nm} is a finite difference approximation for the flux from grid block m into n, given by

$$F_{nm} = k_{nm}\left(\frac{k_{\mathrm{rl}}\,\rho_{\mathrm{l}}}{\mu_{\mathrm{l}}}\right)_{nm}\left(\frac{P_m - P_n}{D_{nm}} + \rho_{\mathrm{l}}\, g_{nm}\right). \tag{8}$$

The subscript nm denotes appropriately weighted quantities pertaining to the interface between grid blocks n and m. D_{nm} is the nodal distance, and g_{nm} is the component of gravitational acceleration along the line from m to n. Q_n is the total sink/source rate in grid block n.

Let us now specialize to a 2-D vertical section with coordinates x (horizontal) and z (vertical), and consider the following simultaneous transformation of space and time coordinates,

$$t \to t' = \lambda_t \cdot t$$

$$x \to x' = \lambda_x \cdot x$$

$$z \to z' = \lambda_z \cdot z. \tag{9}$$

In this paper we strictly limit the discussion to the properties of Richards' equation under the scaling of Eq. (9). We do not address the broader issue of how the scaling of space coordinates may affect the appropriate averaging scales to be used for the definition of hydrologic properties of geologic media. Under the transformation Eq. (9), subdomain volumes V_n scale by $\lambda_x \lambda_z$, so that the coefficient $(\Delta t/V_n)$ in front of flow and sink/source terms in Eq. (6) scales by $\lambda_t/\lambda_x\lambda_z$. Scaling behavior is different for horizontal and vertical areas, and is also different for gravity-driven flow as compared to capillary- or pressure-driven flow. Interface areas A_{nm} for horizontal and vertical flow scale by λ_z and λ_x, respectively. From Eq. (8) it is seen that the gravity (body force) flux term remains unchanged under the scaling Eq. (9), while pressure and capillary-driven fluxes scale with nodal distance D_{nm} as $1/\lambda_x$ and $1/\lambda_z$ for horizontal and vertical components, respectively. The resulting scaling coefficients for horizontal and vertical components of flow terms corresponding to different flow mechanisms are shown in Table 4.

We are interested in determining the conditions, if any, for which Eq. (6) would be invariant under the simultaneous space-and-time scaling of Eq. (9). For an invariance to

Table 4
Scaling coefficients for flow equations

Flow component Flow mechanism	Horizontal	Vertical
Capillarity, pressure	λ_t/λ_x^2	λ_t/λ_z^2
Gravity	–	λ_t/λ_z

hold, the scale factors in Eq. (9) must be chosen in such a way that the scaling coefficients given in Table 4 are all equal to 1. This would assure that changes ΔM_n in the accumulation terms calculated from Eq. (6) would be the same in the scaled as in the original system, grid block for grid block and time step for time step, so that fluid distributions would evolve in identical fashion. Inspection of Table 4 shows that it is not possible to achieve scaling invariance simultaneously for vertical flows under (capillary) pressure and gravity forces. Indeed, the former would demand $\lambda_t/\lambda_z^2 = 1$, whereas the latter would require $\lambda_t/\lambda_z = 1$, which conditions can be satisfied simultaneously only for the trivial case $\lambda_z = 1$. Therefore, generally speaking, flow processes involving these different driving forces will not possess any scaling invariance but will evolve differently on different scales. However, an approximate scaling invariance may still hold when liquids percolate downward in an unsaturated medium of 'relatively high' permeability. In this case (sub-)vertical flows will be primarily driven by gravity, and capillary and pressure effects on vertical flows may be small. An approximate invariance would then be expected to hold when scaling in such a fashion that $\lambda_t/\lambda_x^2 = 1$ and $\lambda_t/\lambda_z = 1$, i.e.,

$$\lambda_t = \lambda_x^2 = \lambda_z. \tag{10}$$

Thus, the vertical length scale and the time scale need to be stretched by the square of the horizontal scale factor. Under the scaling of Eq. (10), vertical flow contributions from capillary and pressure effects would not be invariant, but would change by a factor $\lambda_t/\lambda_z^2 = 1/\lambda_z = 1/\lambda_x^2$. This relationship shows that, if indeed capillary and pressure effects on vertical flows are small in the initial (unscaled) system, they will be even smaller under upscaling ($\lambda_x > 1$). However, under downscaling ($\lambda_x < 1$) these terms will increase in magnitude relative to the gravity term, suggesting that the approximate scaling invariance of Eq. (10) will eventually break down when scaling down to 'sufficiently' small systems.

A number of numerical simulation experiments have been performed to test the approximate scaling invariance postulated in Eq. (10). We applied scale factors of $\lambda_x = 5$ and $1/5$, respectively, simultaneously scaling spatial dimensions and time according to Eq. (10). The spatial scaling changes the 20 m × 20 m heterogeneous fracture of Fig. 2 into 100 m × 500 m ($\lambda_x = 5$) and 4 m × 0.8 m ($\lambda_x = 1/5$),

Table 5
Scaling behavior of simulated seeps

Seep	# 1	# 2	# 3	# 4
Upscaling by $\lambda_x = 5.0$				
Breakthrough time at 487.5 m depth (days)	15.87	14.84	24.95	16.53
Average seepage velocity (m/h)	1.28	1.37	0.81	1.23
Downscaling by $\lambda_x = 0.2$				
Breakthrough time at 0.78 m depth (min)	55.67	51.95	71.65	58.14
Average seepage velocity (m/h)	0.84	0.90	0.65	0.80

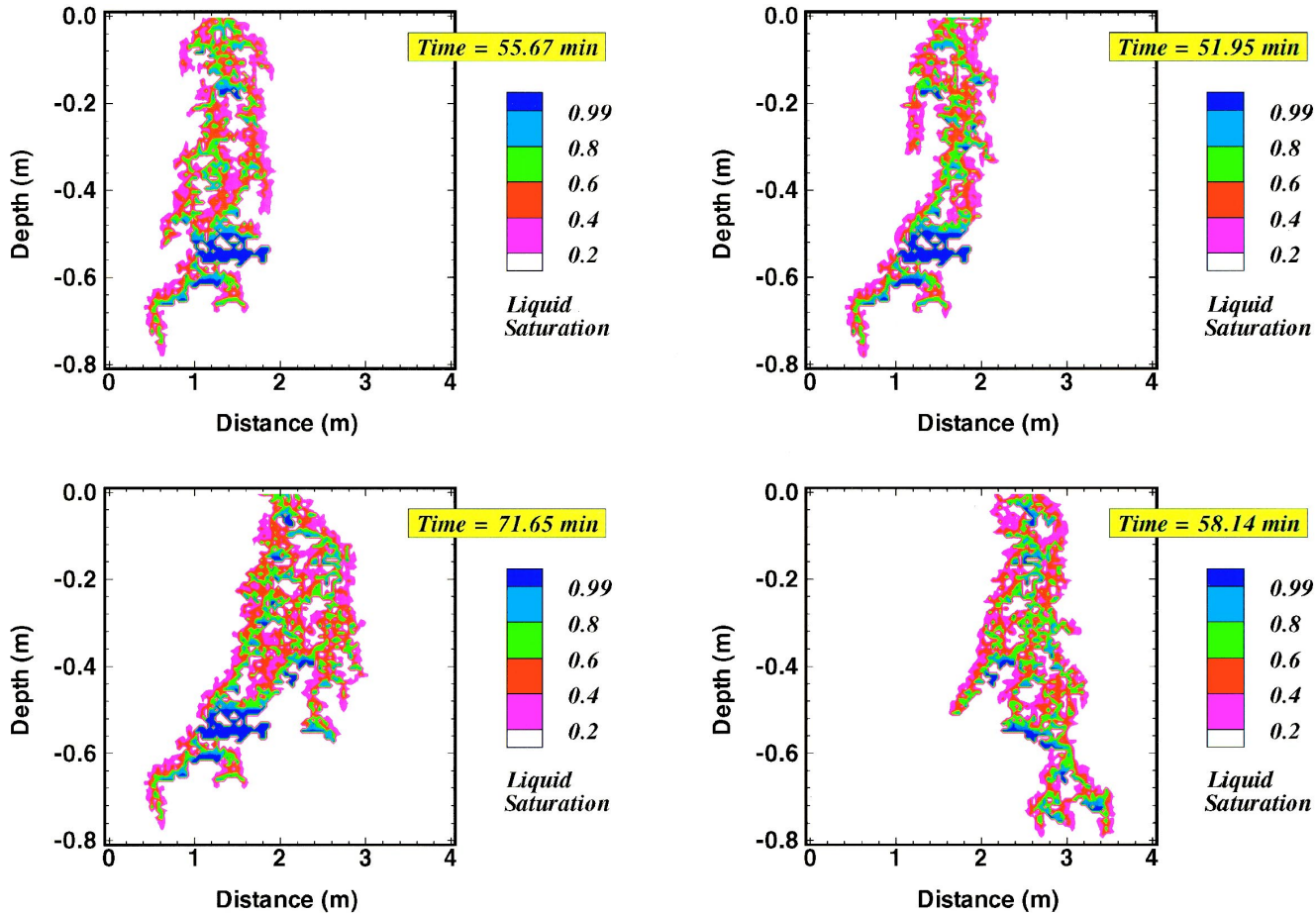

Fig. 14. Liquid seeps shown at the time of breakthrough at a depth of -0.78 m. Water is injected at a constant rate of 0.2×10^{-3} kg/s over a 0.2 m interval at the top of the fracture. The injection interval is centered at different distances from the left boundary, namely, 1.3 m (top left), 1.7 m (top right), 2.1 m (bottom left), and 2.5 m (bottom right). Reference permeability is 10^{-9} m^2.

respectively. Source (injection) rates were scaled by $\lambda_x \lambda_z / \lambda_t = \lambda_x$ (cf. the discussion following Eq. (9)). Upscaling by a factor $\lambda_x = 5$ produces seepage patterns that are so close to the original as to be virtually indistinguishable in all cases. The almost exact mimicking of even small-scale details in saturation distributions between the original and the scaled system demonstrates the excellent validity of the approximate scaling relationship Eq. (10) for this case. This is also borne out by a comparison of the average seepage velocities, see Tables 2 and 5. A different picture emerges for downscaling by a factor of $\lambda_x = 1/5$. Comparison of Fig. 14 with Fig. 5 shows that, while overall seepage patterns are similar, there are very visible and significant differences. Regions of large water saturation tend to be more extensive in the downscaled system, and overall water saturations tend to be larger. This leads to seepage velocities that are typically 30% slower (see Table 5). It is evident that capillary effects on vertical flow have become significant for the small-scale system shown in Fig. 14, so that the scaling relationship Eq. (10) is a rather poor approximation in this case.

9. Validity of scaling invariance

We now attempt to quantify the limitations of the approximate scaling invariance, Eq. (10). Consider gravity-driven seepage in a homogeneous fracture inclined at an angle α relative to the vertical. From Darcy's law, in a fracture with vertical permeability k_{v} the downward advancement of a seep under unit head gradient conditions will proceed with a velocity

$$v = \frac{k_{\mathrm{v}}}{\phi} \frac{\rho_{\mathrm{l}} g \cos\alpha}{\mu_{\mathrm{l}}} \frac{k_{\mathrm{rl}}}{(S_{\mathrm{l}} - S_{\mathrm{lr}})} \tag{11}$$

In writing Eq. (11) we have assumed that the fracture initially is at irreducible water saturation S_{lr}. As the seep advances it is affected by capillary forces. These are diffusive in nature, corresponding to second-order space derivatives in the governing Eq. (2).

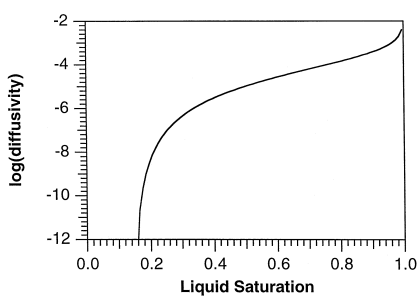

Fig. 15. Unsaturated liquid diffusivity for the parameters used in this study (units of m^2/s).

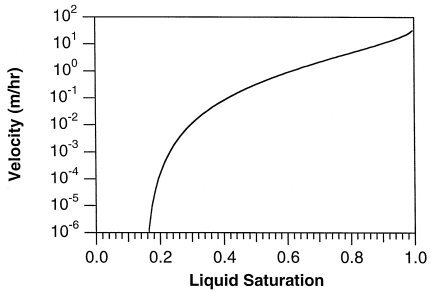

Fig. 16. Advective seep velocity for gravity-driven flow in a vertical fracture of permeability $k_v = 0.36 \times 10^{-9}$ m^2.

Over a time period t, diffusive propagation occurs over a distance (Carslaw and Jaeger, 1959)

$$l = \sqrt{Dt}\,, \tag{12}$$

where

$$D = \frac{k_{ref} k_{rl}}{\phi \mu_l} \frac{\mathrm{d}P_{cap}}{\mathrm{d}S_l} \tag{13}$$

is the effective unsaturated diffusivity at reference permeability k_{ref} (Pruess et al., 1990b). The time required for a seep to advance over a domain of vertical length L is $t = L/v$. The diffusive propagation from capillary effects during this time will be given by

$$l = \sqrt{DL/v}\,. \tag{14}$$

In order for scaling invariance to hold, we require that $l/L \ll 1$, or

$$\frac{l}{L} = \sqrt{\frac{D}{vL}} \ll 1. \tag{15}$$

The group D/vL is an inverse Peclet number. Both diffusivity D and advective velocity

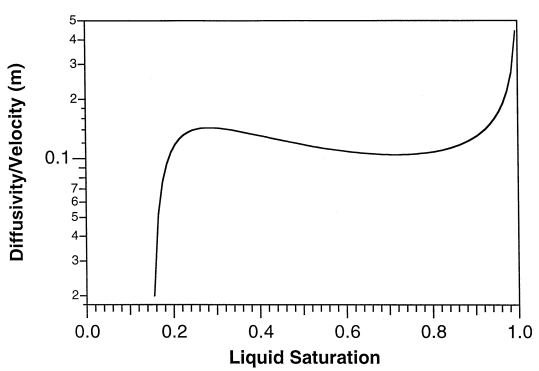

Fig. 17. Ratio of capillary diffusivity to advective velocity.

Table 6
Scale dependence of capillary to gravity effects on seepage

λ_x	L (m)	$l/L = \sqrt{D/vL}$
0.2	0.8	0.371
1	20	0.074
5	500	0.015

v increase strongly with increasing liquid saturation (Figs. 15 and 16). From Eqs. (11) and (13), the group D/v for a vertical fracture is given by

$$\frac{D}{v} = \frac{k_{\mathrm{ref}}}{k_{\mathrm{v}}} \frac{S_{\mathrm{l}} - S_{\mathrm{lr}}}{\rho_{\mathrm{l}} g} \frac{\mathrm{d}P_{\mathrm{cap}}}{\mathrm{d}S_{\mathrm{l}}}, \tag{16}$$

which for the parameters chosen here (see Table 1) is only weakly dependent on saturation in the range $0.2 \leq S_{\mathrm{l}} \leq 0.95$ (Fig. 17). Using a typical (and insensitive) value of $D/v = 0.11$ m at the saturation level of interest, the parameter group of Eq. (15) takes on the values shown in Table 6 for the three scaled fractures. It is seen that the ratio of capillary to gravity effects is small ($l/L \ll 1$) for $\lambda_x = 1$ and 5, but not for $\lambda_x = 0.2$, which explains the observed scale invariance for the former, and the lack of scale invariance for the latter.

The above derivation and discussion emphasized the time-dependent competition between gravity and capillary effects on downward advective flows, and is only applicable to transient behavior. Continued application of infiltration at the top of the fracture, beyond the time required for the seep to break through at the bottom boundary, will cause the seepage pattern to change in ways that will not be invariant under the constraint Eq. (10). Indeed, as steady state is approached time will no longer be a factor, rendering Eq. (10) inapplicable.

The scaling relationship Eq. (10) is applicable for media with self-affine heterogeneity structure, where the heterogeneous permeability fields scale by factors λ_x and $\lambda_z = \lambda_x^2$ in horizontal and vertical directions, respectively. A rigorous scaling of heterogeneous permeability fields may be achieved for a man-made machined specimen, but will, strictly speaking, never be realized for natural fractures. However, many naturally occurring geometries are self-similar or self-affine fractals (Mandelbrot, 1983), and rock fractures may also have such properties (Brown and Scholz, 1985; Wang et al., 1988; Nolte et al., 1989). Heterogeneous fractures on different scales may represent different realizations of the same or a similar heterogeneity structure. Accordingly, for natural fracture systems Eq. (10) should be interpreted in a stochastic rather than a deterministic sense (Miller and Miller, 1956), indicating an approximate invariance 'on average' between transient seepage patterns on different scales.

10. Discussion and conclusions

Recent advances in numerical simulation capabilities have made possible fully transient simulations of two- and three-dimensional unsaturated flow in heterogeneous

media, with detailed resolution of small-scale heterogeneity, and including highly non-linear transitions between partially and fully saturated conditions locally. We have simulated water seepage under different boundary conditions in a small number of heterogeneous fractures, observing a range of behavior. The simulations presented here were exploratory in nature; more diverse heterogeneity structures and a much larger number of stochastic realizations should be studied in the future to more fully explore the behavior of seeps and determine their statistical features.

Our limited number of simulations of infiltration in synthetic heterogeneous fractures has demonstrated many of the features seen in naturally fractured systems in thick unsaturated zones, such as Yucca Mountain and Rainier Mesa, Nevada, including fast preferential flow, flow fingering, bypassing, and ponding. Seepage along highly localized flow paths is of particular concern in connection with waste isolation in thick unsaturated zones, as it can give rise to fast transport of solutes even under conditions where average net infiltration is very small (a few millimeters per year).

We find that 'fast' flow can be generated by either 'internal' or 'external' mechanisms, or combinations thereof. 'Internal' enhancement of seepage velocities occurs from seepage exclusion and flow funnelling due to medium heterogeneities. Features of low effective permeability, such as capillary barriers, fracture terminations, or asperity contacts in fractures may exclude flow from certain regions, while concentrating it into others. The effectiveness of sub-horizontal barriers in enhancing downward seepage velocities increases with their lateral extent. 'External' enhancement occurs from localized preferential infiltration at the land surface boundary. This may be caused by topographic relief and associated runoff, which may funnel and focus much infiltration into topographic lows, leading to locally enhanced seepage which may persist to depth. Also, fractures or faults extending to the land surface may accept an above-average amount of infiltration. Our numerical simulations have shown that each of these mechanisms is easily capable of enhancing seepage (pore) velocities by factors of 5–10 in comparison with uniform infiltration in homogeneous fractures. We expect that considerably larger velocity enhancements can be generated in funnel-like land surface or subsurface structures of larger areal extent.

Observations of environmental tracers at Yucca Mountain indicate solute transport velocities of order 10 m/yr (Fabryka-Martin et al., 1996). At an estimated average net infiltration rate of a few millimeters per year (Flint et al., 1996), and an average total porosity of approximately 10%, this corresponds to a seepage velocity enhancement by factors of a few hundred relative to uniform infiltration in a homogeneous medium. Our results suggest that a combination of internal and external flow funneling mechanisms can easily account for such enhancements.

Sub-horizontal barriers diminish average permeability in the vertical direction, but may cause large enhancements in downward seepage velocity. A remarkable finding from our simulations is that unsaturated seepage may actually proceed faster in media with lower average permeability. Our results show that seepage in unsaturated heterogeneous media has many features that cannot be understood or approximated in terms of volume-averaged homogenized models.

Infiltration into partially saturated heterogeneous media can give rise to a variety of behavior, from localized seeps to broad plumes with dispersed flow at some depth

beneath the infiltration region. Field experiments have frequently shown flow focusing or funneling into fast preferential pathways (Kung, 1990a,b). However, this type of behavior is by no means universal or inevitable. Depending on the nature and spatial scale of heterogeneity the opposite effect—transverse spreading of descending infiltration plumes—is also possible (Pruess, 1996b). More work is needed to explore heterogeneity conditions for which spatially-distributed infiltration could give rise to highly localized preferential flows.

An approximate invariance of seepage under simultaneous space-and-time scaling was theoretically derived. The validity and limitations of this invariance were demonstrated through numerical simulations, and through analyses of capillary- and gravity-driven flows. The scaling behavior suggests that, in fractured media with 'sufficiently' high permeability, transient seeps should show a more vertically elongated appearance as the scale of observation increases.

Future experimental and numerical studies should investigate different types of heterogeneity structures, such as three-dimensional fracture networks, and a variety of boundary and source conditions, including non-uniform, localized infiltration at time-varying rates. Of interest is also the interaction between seeps, and seepage behavior over longer time scales, subject to interaction between fractures and matrix rock, as well as to a number of subtle multi-phase effects.

Acknowledgements

This work was supported, in part, by the Director, Office of Civilian Radioactive Waste Management, and by the Director, Office of Energy Research, Office of Health and Environmental Sciences, Biological and Environmental Research Program, of the U.S. Department of Energy under Contract No. DE-AC03-76SF00098. Thanks are due to Emilio Antunez for assistance with the generation of spatially correlated stochastic fields, and to Jil Geller, Boris Faybishenko, and Stefan Finsterle for a review of the manuscript and the suggestion of improvements. Helpful discussions with Curt Oldenburg are gratefully acknowledged. The paper benefitted from valuable suggestions made in the review process by G. de Marsily, J.P. Hulin, and an anonymous reviewer.

References

Abelin, H., Birgersson, L., Gidlund, J., Moreno, L., Neretnieks, I., Tunbrant, S., 1987. Results from some tracer experiments in crystalline rocks in Sweden. In: Tsang, C.F. (Ed.), Coupled Processes Associated with Nuclear Waste Respositories. Academic Press, New York, 1987.

Birkholzer, J., Tsang, C.F., 1996. Solute channeling in unsaturated heterogeneous porous media, 1996. Submitted to Water Resour. Res.

Brown, S.R., Scholz, C.H., 1985. Broad bandwidth study of the topography of natural rock surfaces. J. Geophys. Res. 90, 12575–12582.

Carslaw, H.S., Jaeger, J.C., 1959. Conduction of Heat in Solids, 2nd edn. Oxford Univ. Press, Oxford, England.

Chesnut, D.A., 1992. Characterizing the altered zone at yucca mountain: The beginning of a testing strategy.

Proceedings, Third High Level Radioactive Waste Management International Conference, Las Vegas, NV, Vol. 1, pp. 1026–1039, American Nuclear Society, La Grange Park, IL, April 12–16, 1992.

Chesnut, D.A., 1994. Dispersivity in heterogeneous permeable media. Proceedings, Fifth Annual International High-Level Radioactive Waste Management Conference, Las Vegas, NV, Vol. 4, pp. 1822–1841, American Nuclear Society, La Grange Park, IL, May 1994.

Eaton, R.R., Ho, C.K., Glass, R.J., Nicholl, M.J., Arnold, B.W., 1996. Modeling of flow through fractured tuff at Fran Ridge. Proceedings, Seventh Annual International High-Level Radioactive Waste Management Conference, Las Vegas, NV, pp. 76–78, American Nuclear Society, La Grange Park, IL, April 1996.

Fabryka-Martin, J., Wolfsberg, A.V., Dixon, P.R., Levy, S., Musgrave, J., Turin, H.J., 1996. Summary report of chlorine-36 studies: Sampling, analysis and simulation of chlorine-36 in the exploratory studies facility. Los Alamos National Laboratory Report LA-CST-TIP-96-002, Los Alamos, NM 87545, August 1996.

Firoozabadi, A., Hauge, J., 1990. Capillary pressure in fractured porous media, J. Pet. Technol., June 1990, 784–791.

Flint, A., Hevesi, J.A., Flint, L.E., 1996. Conceptual and numerical model of infiltration for the Yucca Mountain area, NV. Water Resources Investigation Report, U.S. Geological Survey, Denver, CO, 1996.

Gauthier, J.H., 1994. An updated fracture flow model for total-system performance assessment of Yucca Mountain. Proceedings, Fifth Annual International High-Level Radioactive Waste Management Conference, Las Vegas, NV, Vol. 3, pp. 1663–1670, American Nuclear Society, La Grange Park, IL, May 1994.

Gauthier, J.H., Wilson, M.L., Lauffer, F.C., 1992. Estimating the consequences of significant fracture flow at Yucca Mountain. Proceedings, Third Annual International High-Level Radioactive Waste Management Conference, Las Vegas, NV, Vol. 1, pp. 891–898, American Nuclear Society, La Grange Park, IL, April 1992.

Geller, J., Pruess, K., 1995. On water infiltration in rough-walled fractures. Proceedings, Sixth Annual International High-Level Radioactive Waste Management Conference, Las Vegas, NV, pp. 23–25, American Nuclear Society, La Grange Park, IL, May 1995.

Glass, R.J., 1993. Modeling gravity-driven fingering in rough-walled fractures using modified percolation theory. Fourth Annual International High-Level Radioactive Waste Management Conference, Las Vegas, NV, pp. 2042–2052, American Nuclear Society, La Grange Park, IL, April 1993.

Kung, K.J.S., 1990a. Preferential flow in a sandy vadose zone: 1. Field observation. Geoderma 46, 51–58.

Kung, K.J.S., 1990b. Preferential flow in a sandy vadose zone: 2. Mechanism and implications. Geoderma 46, 59–71.

Lawrence Berkeley Laboratory, 1991. Geologic repository project, a review of Rainier Mesa Tunnel and borehole data and their possible implications to Yucca Mountain Site study plans. Lawrence Berkeley Laboratory Report LBL-32068, December 1991, 99 pp.

Leverett, M.C., 1941. Capillary behavior in porous solids. Trans. Soc. Pet. Eng. AIME 142, 152–169.

Mandelbrot, B.B., 1983. The Fractal Geometry of Nature. Freeman, New York, NY.

Miller, E.E., Miller, R.D., 1956. Physical theory for capillary flow phenomena. J. Appl. Phys. 27 (4), 324–332.

Moridis, G., Pruess, K., 1995. Flow and transport simulations using T2CG1, a package of conjugate gradient solvers for the TOUGH2 family of codes. Lawrence Berkeley Laboratory Report LBL-36235, Lawrence Berkeley Laboratory, Berkeley, CA, 1995.

Nativ, R., Adar, E., Dahan, O., Geyh, M., 1995. Water recharge and solute transport through the vadose zone of fractured chalk under desert conditions. Water Resour. Res. 31 (2), 253–261.

Nicholl, M.J., Glass, R.J., Nguyen, H.A., 1993. Wetting front instability in an initially wet unsaturated fracture. Proceedings, Fourth High Level Radioactive Waste Management International Conference, Las Vegas, NV, April 26–30, 1993.

Nicholl, M.J., Glass, R.J., Wheatcraft, S.W., 1994. Gravity-driven infiltration instability in initially dry nonhorizontal fractures. Water Resour. Res. 30 (9), 2533–2546.

Nitao, J.J., Buscheck, T.A., 1991. Infiltration of a liquid front in an unsaturated, fractured porous medium. Water Resour. Res. 27 (8), 2099–2112.

Nolte, D.D., Pyrak-Nolte, L.J., Cook, N.G.W., 1989. The fractal geometry of the flow paths in natural fractures in rock and the approach to percolation. Pageoph. 131 (1/2), 111–138.

Oldenburg, C.M., Pruess, K., 1993. On numerical modeling of capillary barriers. Water Resour. Res. 29 (4), 1045–1056.

Persoff, P., Pruess, K., 1995. Two-phase flow visualization and relative permeability measurement in natural rough-walled rock fractures. Water Resour. Res. 31 (5), 1175–1186.

Peters, R.R., Klavetter, E.A., 1988. A continuum model for water movement in an unsaturated fractured rock mass. Water Resour. Res. 24 (3), 416–430.

Peters, R.R., Klavetter, E.A., Hall, I.J., Blair, S.C., Heller, P.R., Gee, G.W., 1984. Fracture and matrix hydrologic characteristics of tuffaceous materials from Yucca Mountain, Nye County, NV. Report SAND84-1471, Sandia National Laboratories, Albuquerque, NM, December 1984.

Pruess, K., 1991. TOUGH2—A general purpose numerical simulator for multiphase fluid and heat flow. Report No. LBL-29400, Lawrence Berkeley Laboratory, Berkeley, CA, May 1991.

Pruess, K., 1994. On the validity of a Fickian diffusion model for the spreading of liquid infiltration plumes in partially saturated heterogeneous media. Computational Methods in Water Resources X, Vol. 1. Kluwer Academic Publishers, Dordrecht, pp. 537–544.

Pruess, K., 1996. Effective parameters, effective processes: From porous flow physics to in situ remediation technology. In: Kobus, H., Barczewski, B., Koschitzky, H.P. (Eds.), Groundwater and Subsurface Remediation. Springer, Berlin, pp. 183–193.

Pruess, K., 1996b. A Fickian diffusion model for the spreading of liquid plumes infiltrating in heterogeneous media. Transport in Porous Media 24 (1), 1–33.

Pruess, K., 1996. Numerical simulation experiments on water seepage patterns in heterogeneous, unsaturated rock fractures. Lawrence Berkeley National Laboratory Report LBNL-38883, Berkeley, CA, May 1996.

Pruess, K., Antunez, E., 1995. Applications of TOUGH2 to infiltration of liquids in media with strong heterogeneity. Proceedings of the TOUGH Workshop '95, Lawrence Berkeley Laboratory Report LBL-37200, Berkeley, CA, March 1995, pp. 69–76.

Pruess, K., Tsang, Y.W., 1990. On two-phase relative permeability and capillary pressure of rough-walled rock fractures. Water Resour. Res. 26 (9), 1915–1926.

Pruess, K., Wang, J.S.Y., Tsang, Y.W., 1990a. On thermohydrological conditions near high-level nuclear wastes emplaced in partially saturated fractured tuff: Part 1. Simulation studies with explicit consideration of fracture effects. Water Resour. Res. 26 (6), 1235–1248.

Pruess, K., Wang, J.S.Y., Tsang, Y.W., 1990b. On thermohydrological conditions near high-level nuclear wastes emplaced in partially saturated fractured tuff: Part 2. Effective continuum approximation. Water Resour. Res. 26 (6), 1249–1261.

Thordarson, W., 1965. Perched groundwater in zeolitized-bedded tuff, Rainier Mesa and vicinity, Nevada test site, NV. U.S. Geological Survey Report TEI-862, 93 pp.

Tompson, A.F.B., 1989. Implementation of the three-dimensional turning bands random field generator. Water Resour. Res. 25 (10), 2227–2243.

Tsang, Y.W., Tsang, C.F., 1987. Channel model of flow through fractured media. Water Resour. Res. 23 (3), 467–479.

van Genuchten, M.Th., 1980. A closed-form equation for predicting the hydraulic conductivity of unsaturated soils. Soil Sci. Soc. Am. J. 44, 892–898.

Wang, J.S.Y., Narasimhan, T.N., 1985. Hydrologic mechanisms governing fluid flow in a partially saturated, fractured, porous medium. Water Resour. Res. 21 (12), 1861–1874.

Wang, J.S.Y., Narasimhan, T.N., 1993. Unsaturated flow in fractured porous media. In: Flow and Contaminant Transport in Fractured Rock. Academic Press.

Wang, J.S.Y., Narasimhan, T.N., Scholz, C.H., 1988. Aperture correlation of a fractal fracture. J. Geophys. Res. 93 (B3), 2216–2224.

Wang, J.S.Y., Cook, N.G.W., Wollenberg, H.A., Carnahan, C.L., Javandel, I., Tsang, C.F., 1993. Geohydrologic data and models of Rainier Mesa and their implications to Yucca Mountain. Proceedings, Fourth Annual International High-Level Radioactive Waste Management Conference, Las Vegas, NV, Vol. 1, pp. 675–681, American Nuclear Society, La Grange Park, IL, April 1993.

Witherspoon, P.A., Wang, J.S.Y., Iwai, K., Gale, J.E., 1980. Validity of cubic law for fluid flow in a deformable rock fracture. Water Resour. Res. 16 (6), 1016–1024.

Yang, I.C., Rattray, G.W., Yu, P., 1995. Chemical and isotopic data and interpretations, unsaturated zone boreholes, Yucca Mountain, NV. Water Resources Investigation Report, U.S. Geological Survey, Denver, CO, 1995.